THE JOURNAL OF PHYSICAL CHEMISTRY C

Article

pubs.acs.org/JPCC

Energy Loss Function of Solids Assessed by Ion Beam Energy-Loss Measurements: Practical Application to Ta_2O_5

Raul C. Fadanelli,[†] Moni Behar,[†] Luiz C. C. M. Nagamine,[‡] Maarten Vos,[§] Néstor R. Arista,[∥] Chiara D. Nascimento,[†] Rafael Garcia-Molina,[⊥] and Isabel Abril*[,#]

[†]Laboratório de Implantação Iônica, Instituto de Física, Universidade Federal do Rio Grande do Sul, Porto Alegre 91501-970, Brazil

[‡]Instituto de Física, Universidade de São Paulo, 05508-090 São Paulo, São Paulo, Brazil

[§]Atomic and Molecular Physics Laboratories, Research School of Physics and Engineering, Australian National University, Canberra 0200, Australia

[∥]Centro Atómico Bariloche and Instituto Balseiro, Comisión Nacional de Energía Atómica, 8400 San Carlos de Bariloche, Argentina

[⊥]Departamento de Física − Centro de Investigación en Óptica y Nanofísica, Regional Campus of International Excellence "Campus Mare Nostrum", Universidad de Murcia, E-30100 Murcia, Spain

[#]Departament de Física Aplicada, Universitat d'Alacant, E-03080 Alacant, Spain

ABSTRACT: We present a study where the energy loss function of Ta_2O_5, initially derived in the optical limit for a limited region of excitation energies from reflection electron energy loss spectroscopy (REELS) measurements, was improved and extended to the whole momentum and energy excitation region through a suitable theoretical analysis using the Mermin dielectric function and requiring the fulfillment of physically motivated restrictions, such as the *f*- and KK-sum rules. The material stopping cross section (SCS) and energy-loss straggling measured for 300−2000 keV proton and 200−6000 keV helium ion beams by means of Rutherford backscattering spectrometry (RBS) were compared to the same quantities calculated in the dielectric framework, showing an excellent agreement, which is used to judge the reliability of the Ta_2O_5 energy loss function. Based on this assessment, we have also predicted the inelastic mean free path and the SCS of energetic electrons in Ta_2O_5.

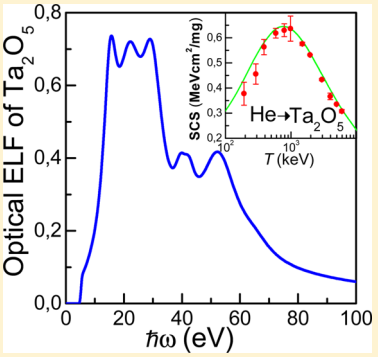

I. INTRODUCTION

The electronic excitation spectrum of a solid is a basic input in materials science, either to gain knowledge from the fundamental point of view, to improve analysis and characterization techniques or to foster new applications.[1−3] This excitation spectrum often appears encoded in the energy loss function (ELF), which provides a complete description of the response of the medium to an external electromagnetic perturbation.[4] Reliable excitation spectra are required in order to take into account the phase and chemical effects that unavoidably appear when working in solids.

There are several methods to derive the ELF, which are based on experimental measurements,[5−10] or theoretical considerations,[11−14] but the information provided by the former rarely covers the whole (or a sufficiently broad) electronic excitation energy and momentum region, whereas the theoretical calculations many times lack of a direct experimental assessment.

We present a joint experimental-theoretical study where the excitation spectrum of Ta_2O_5 measured by reflection electron energy loss spectroscopy (REELS), which only covers a small region (optical, i.e., zero momentum transfer, and valence electron excitations), is improved and extended to the whole excitation region through a suitable theoretical analysis that requires the fulfillment of physically motivated sum rules[15] and includes the contribution of intermediate and inner shell excitations. The resulting ELF is used as input for the dielectric formalism to evaluate the energy loss magnitudes characterizing the passage of swift ions through matter. These calculations are compared with the measured stopping cross section and energy-loss straggling of Ta_2O_5 films for proton and helium ion beams by means of Rutherford backscattering spectrometry. The excellent agreement between the experimental and theoretical results is used as an assessment of the derived energy loss function for Ta_2O_5.

Due to its high dielectric constant, chemical and thermal stability, as well as wear resistance, tantalum oxide (Ta_2O_5) is a promising material for solar energy conversion systems, CMOS-based technology and resistive random access memories.[16−19] Therefore, it is important to have a proper knowledge of the electronic excitation spectrum of this material, which is provided in this work as previously described.

This paper is organized as follows. In section II, the energy loss function of Ta_2O_5 in the optical limit (zero momentum transfer, $\hbar k = 0$) is derived from REELS measurements. This energy loss function is extended in section III to the whole

Received: May 5, 2015
Revised: July 31, 2015

DOI: 10.1021/acs.jpcc.5b04292
J. Phys. Chem. C XXXX, XXX, XXX−XXX

energy ($\hbar\omega$) and momentum ($\hbar k$) transfers region by using the Mermin-energy-loss function and generalized oscillator strength (MELF-GOS) method. Section IV is devoted to the calculation of the Ta_2O_5 stopping cross section and energy-loss straggling by means of the dielectric formalism. The measurement of these characteristic energy loss magnitudes for proton and helium ion beams and the comparison with the theoretical predictions are presented in section V. The excellent agreement between experiments and theory give us confidence to compute the stopping cross sections and the inelastic mean free path of energetic electrons in Ta_2O_5 films, which are presented in section VI. Finally, the summary and conclusions of this work are outlined in section VII.

II. ELECTRONIC EXCITATION SPECTRUM OF Ta_2O_5 FROM REELS MEASUREMENTS

Despite the importance of the electronic excitation spectrum of a material such as Ta_2O_5, no experimental data are available for it in a wide range of excitation energies $\hbar\omega$. There are transmittance and spectro-photometric measurements in a wavelength range that only allows obtaining the refractive and absorptive index for energies less than 6 eV.[20−22] From experimental ellipsometry data, Franke et al.[23] got the dielectric function of Ta_2O_5 thin films in the spectral region 0.03−8.5 eV. Reflection electron energy loss measurements are an established way of determining the energy loss function of a material,[1,24] and the spectrum of amorphous Ta_2O_5 for 200 eV electrons has been measured up to 60 eV energy losses, but being expressed in arbitrary units it is not an immediate task to obtain the energy loss function.[25]

In what follows, we present experimental data of the energy loss function of Ta_2O_5 extracted from REELS measurements at higher incident electron energies, ranging from 5 to 40 keV, and with good energy resolution (0.3 eV). These experiments were performed at the Atomic and Molecular Physics Laboratories of the Australian National University. We studied a Ta sample on which a 50 nm thick Ta_2O_5 layer was grown by thermal oxidation (600 °C for 30 min under a 100 standard cubic centimeters per minute O_2 flow). The measurements (with the elastic peak normalized to unit area) are shown in the upper panel of Figure 1 for 5 and 40 keV incident electron beams. The spectra consist of electrons that were detected after zero (i.e., elastic peak) and one or more inelastic events. The feature in the 40 keV spectrum appearing at 4 eV energy loss is due to electrons scattered elastically from oxygen, as the recoil energy loss of a 40 keV electron scattered over 135° is resolved in this experiment. The intensity and position of this feature are linked to the intensity and position of the main elastic peak, which is due to electrons scattered from Ta. As explained elsewhere,[26] it is possible to remove this feature, that is, correct the spectrum for the electrons scattered from O. The solid line in Figure 1a represents the REELS energy spectrum after subtraction of the intensity due to electrons scattered elastically from O. At the 5 keV electron beam, the recoil energy is not resolved and subtraction of the O-related intensity is not required.

Under quite general assumptions, the (single inelastic scattering) energy loss function (ELF) corresponding to the bulk target (i.e., avoiding surface effect contributions) can be extracted from these experimental data using a procedure described in ref 27. Figure 1b shows the ELF of Ta_2O_5 derived from the REELS measurements presented in the upper panel. The normalized energy loss spectrum is a "weighted sum" of

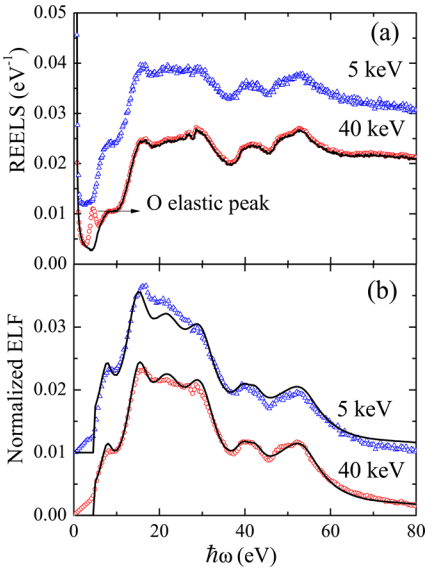

Figure 1. (a) Measured REELS energy spectrum (symbols) in Ta_2O_5 films for incident electron energies of 5 and 40 keV. A separate O elastic peak can be seen for electrons at 40 keV, and after removing it we obtain the black line. (b) Normalized optical energy loss function of Ta_2O_5 (symbols) for both incident electron energies, and the corresponding fits obtained using the QUEELS package[28] (solid lines). For clarity, the data corresponding to 5 keV electrons are offset by 0.01 in both panels.

surface and bulk electronic excitations. The surface excitation probabilities decrease with increasing incident electron energy. These surface excitations are the cause that the intensity of the normalized energy loss function is larger at 5 keV than at 40 keV for energy losses < 20 eV. The QUEELS package[28] was used to calculate the normalized differential inverse inelastic mean free path (DIIMFP) for electrons. The (unnormalized) electron DIIMFP $W(\omega,T)$ is related to the dielectric function $\varepsilon(k,\omega)$ by

$$W(\omega, T) = \frac{me^2}{\hbar\pi T}\int_{k_1}^{k_2}\frac{dk}{k}\mathrm{Im}\left[\frac{-1}{\varepsilon(k,\omega)}\right] \quad (1)$$

where T is the energy of the incoming electron, m and e represent the electron mass and charge, respectively, and the integration limits $k_{1,2} = ((2m)^{1/2}/\hbar)[\sqrt{T} \mp (T - \hbar\omega)^{1/2}]$ result from energy and momentum conservation in the interaction process.

The target energy loss function, $\mathrm{Im}(-1/\varepsilon)$, is expressed as a set of Drude oscillators such that $W(\omega,T)$ fits the 40 keV spectrum, namely,

$$\begin{aligned}\mathrm{Im}\left[\frac{-1}{\varepsilon(k=0,\omega)}\right]_{\mathrm{REELS}} &= \sum_i A_i \mathrm{Im}\left[\frac{-1}{\varepsilon_{\mathrm{Drude}}(\omega_i,\gamma_i;k=0,\omega)}\right] \\ &= \sum_i A_i \frac{\omega\gamma_i}{(\omega_i^2-\omega^2)^2+(\omega\gamma_i)^2}, \quad \text{for } \omega \geq \omega_{\mathrm{th},i}\end{aligned} \quad (2)$$

where A_i, ω_i, and γ_i are parameters that determine the intensity, position, and width of each Drude oscillator and $\omega_{\mathrm{th},i}$ is a threshold energy. Using these parameters as derived from the 40 keV measurements, one can calculate the 5 keV spectrum in

DOI: 10.1021/acs.jpcc.5b04292
J. Phys. Chem. C XXXX, XXX, XXX−XXX

the QUEELS package. Indeed the calculated 5 keV spectrum from the ELF has an increased intensity for energy losses less than 20 eV, but the changes are not reproduced fully quantitatively, which can be attributed to a possible failure of the momentum dependence of the loss function in the Drude model used.

Therefore, the 40 keV measurement was used to parametrize the ELF rather than the 5 keV ones. First, the surface excitations contribution is small, hence they can be easily avoided. Second, measurements at higher incoming energy have a lower momentum transfer cutoff. Indeed, due to the nature of the Coulomb interaction the ELF is dominated by very low-k losses near the cutoff and the ELF approaches the loss function in the optical limit more and more with increasing incoming energy. Thus, assumptions made about the dispersion (e.g., in the Drude model) become less of a factor at higher energy for the derivation of the energy loss function in the optical limit.

As from the REELS experiment one obtains only the shape of the optical energy loss function, one has to set the ELF in eq 2 on an absolute scale. For this purpose, QUEELS uses the Kramers–Kronig (KK) sum rule:[29,30]

$$\frac{2}{\pi}\int_0^\infty \frac{1}{\omega}\mathrm{Im}\left[\frac{-1}{\varepsilon(k=0,\omega)}\right]\mathrm{d}\omega = 1 - \frac{1}{n(0)^2} \tag{3}$$

where $n(0)$ represents the refractive index at the static limit ($\omega \to 0$). Therefore, it is necessary to rescale the parameters A_i in the set of Drude oscillators, used to describe the ELF through eq 2, in such a way that the KK sum rule will be fulfilled. For this we need the refractive index value of Ta_2O_5 as input, which has been taken to be $n(0) = 1.75$.[31]

In Table 1, we show the parametrization, with nine Drude oscillators in eq 2, used to describe the outer-shell electrons

Table 1. Parameters Used to Fit the Outer-Shell Electron Contributions to the Optical ELF of Ta_2O_5 Deduced from REELS Experiments

i	$\hbar\omega_i$ (eV)	$\hbar\gamma_i$ (eV)	A_i (eV^2)
1	8	3.5	4.23
2	15.5	6	43.3
3	22.5	11	123
4	30	9	131
5	39.5	5	25.8
6	42.5	5	25.8
7	52	16	240
8	54	8	37.7
9	80	30	94.1

contribution to the optical ELF of Ta_2O_5 obtained from the REELS measurements. The value we have used for $\hbar\omega_{\mathrm{th},i}$ is the gap energy of Ta_2O_5, which is 5 eV.[32]

III. IMPROVING THE ELF THROUGH THE MELF-GOS METHOD

The ELF derived previously from REELS measurements only accounts for contributions of the target outer-shell electrons ($\hbar\omega \leq 80$ eV) to optical (i.e., $k = 0$) excitations. In what follows, we use the MELF-GOS (Mermin energy loss function–generalized oscillator strength) method[11,12,33] to obtain an ELF that covers the whole momentum and energy transfers region. The reliability of this procedure is supported by its successful application to describe properly the electron excitation spectra of elemental and compound targets.[12,34−36] It is worth mentioning that alternate procedures to derive suitable dielectric properties of solids from experimental data have been recently published.[10,37]

The contributions to the target ELF of the outer electron excitations and of the inner-shell ionizations can be explicitly separated as

$$\mathrm{Im}\left[\frac{-1}{\varepsilon(k,\omega)}\right] = \mathrm{Im}\left[\frac{-1}{\varepsilon(k,\omega)}\right]_{\mathrm{outer}} + \mathrm{Im}\left[\frac{-1}{\varepsilon(k,\omega)}\right]_{\mathrm{inner}} \tag{4}$$

The inner-shell electrons have large binding energies, showing a marked atomic character and no collective effects; therefore, they can be suitably modeled by means of the atomic generalized oscillator strengths (GOS), where hydrogenic wave functions are employed with effective nuclear charges for each shell given by Slater's rules. The advantage of this procedure is that analytical expressions for the ELF are available for the nonrelativistic hydrogenic GOS[12]

$$\mathrm{Im}\left[\frac{-1}{\varepsilon(k,\omega)}\right]_{\mathrm{inner}} = \frac{2\pi N}{\omega}\sum_j \alpha_j \sum_{nl}\frac{\mathrm{d}f_{nl}^{(j)}(k,\omega)}{\mathrm{d}\omega} \tag{5}$$

where N is the molecular density of the target, $\mathrm{d}f_{nl}^{(j)}(k,\omega)/\mathrm{d}\omega$ is the hydrogenic GOS corresponding to the (n,l)-subshell of the jth element of the compound target, and α_j indicates its stoichiometric contribution to the compound formula. For Ta_2O_5, the electrons from the K-shell of O, as well as the K-, L-, and M-shells of Ta are treated as inner electrons and described by the GOS.

The electronic excitations of the weakly bound outer shells are described by fitting the experimentally obtained optical ELF, that is, at $k = 0$, by a linear combination of Mermin-type ELFs. For this purpose, we use a similar expression to eq 2, but replacing the Drude dielectric functions by Mermin dielectric functions.[38] The values of the parameters A_i, ω_i, and γ_i are, in principle, the same as those that appear in Table 1, since in the optical limit (i.e., at zero momentum transfer) the Drude and the Mermin ELF are identical;[33] however, in what follows, these parameters will be modified in order to improve the ELF.

The differences between both models (Drude and Mermin) to describe the ELF of a target will appear for momentum transfers different from zero, because an important advantage of the MELF-GOS method is that the fit of the ELF in the optical limit ($k = 0$) is analytically extended to nonzero momentum transfer ($k \neq 0$) through the properties of the Mermin dielectric function.

Besides a good fitting, the constructed ELF must fulfill physically motivated sum rules.[15,30] The Kramers–Kronig (or perfect screening) sum-rule eq 3, already imposed when obtaining the parameters that appear in Table 1, is an important test for the accuracy of the fitted ELF at low energy transfer. But the f-sum rule (or Thomas–Reiche–Kuhn sum rule), which links the ELF to the number of target electrons per molecule that can be excited by the projectile, must also be satisfied for a good behavior of the ELF at intermediate and high energy transfers. It is given by[15,29,30]

$$Z_2 = \frac{m}{2\pi^2 e^2 N}\int_0^\infty \omega\mathrm{Im}\left[\frac{-1}{\varepsilon(k=0,\omega)}\right]\mathrm{d}\omega \tag{6}$$

where Z_2 is the total nuclear charge of the molecule.

DOI: 10.1021/acs.jpcc.5b04292
J. Phys. Chem. C XXXX, XXX, XXX−XXX

Although the experimental ELF of Ta_2O_5 obtained from REELS fulfills the KK-sum rule, eq 3, however the *f*-sum rule is not verified, because using $\mathrm{Im}(-1/\varepsilon)$ in eq 6 with the parameters of Table 1 gives 92.8 electrons for Ta_2O_5, which is far from the right value of 186. Therefore, a new fitting of the Ta_2O_5 optical ELF must be made following the guideline that at low energy transfers it must reproduce the optical ELF obtained from REELS measurements, whereas at intermediate and high excitation energies, where no experimental optical ELF values for Ta_2O_5 are available, it must account for the inner-shell electron contributions to the ELF. For compound targets, as is the case of Ta_2O_5, this contribution is obtained by applying the additivity of the ELF/*N* ratios corresponding to their elementary constituents.[39] Besides the good agreement with experimental data and the fulfillment of the sum rules, the accuracy of the ELF derived from the MELF-GOS methodology relies in the excellent agreement[40,41] with the (scarce) experimental data available for nonzero momentum transfer ELF.

Proceeding in this manner, we have derived an improved ELF that verifies the *f*-sum rule using the parameters given in Table 2, which reproduces the ELF obtained from the REELS data for low-energy transfers and includes the generalized oscillator strengths for high-energy transfers. This new ELF fulfills the *f*-sum rule within 3% and the KK-sum rule better than 4%, the latter value being comparable with the one obtained from the ELF derived from REELS measurements. This improved ELF for Ta_2O_5, depicted in Figure 2 by a blue solid line, coincides for $\hbar\omega \leq 60$ eV with the ELF derived from the REELS data (depicted by a magenta dash-dotted line). At intermediate and high energy transfers the ELF is obtained by the addition of the outer and the inner-shell electron excitations, eq 4, where the last contribution is calculated using the GOS model, according to eq 5. This ELF compares fairly well to the one deduced from the atomic scattering factors at low-intermediate[42] and high[43−45] energies, respectively, depicted by a light[42] or a dark[43−45] gray dashed line.

In Figure 2, we also show, by a magenta dash-dotted line, the optical ELF of Ta_2O_5 built from eq 4, where the outer (least-bound) electron excitation contribution is obtained from eq 2, with the parameters resulting from the REELS measurements, which are given in Table 1, and where the inner-shell contribution is also included. The measurements by Franke et al.[23] at very low transferred energies are depicted by orange dots.

Table 2. New Parameters Used to Improve the Optical ELF of Ta_2O_5 from REELS Measurements When Both the *f*- and the KK-Sum Rules Are Fulfilled[a]

i	$\hbar\omega_i$ (eV)	$\hbar\gamma_i$ (eV)	A_i (eV^2)
1	15.5	5.44	39.24
2	22.5	11	119.95
3	30	9	125.87
4	39.5	5	22.21
5	42.5	5	22.21
6	53.1	16	259.15
7	65.3	13.6	37.02
8	76.2	81.6	222.13
9	163.3	408.2	1236.53

[a]The value $\hbar\omega_{th,i}$ = 5 eV has been used in all cases.

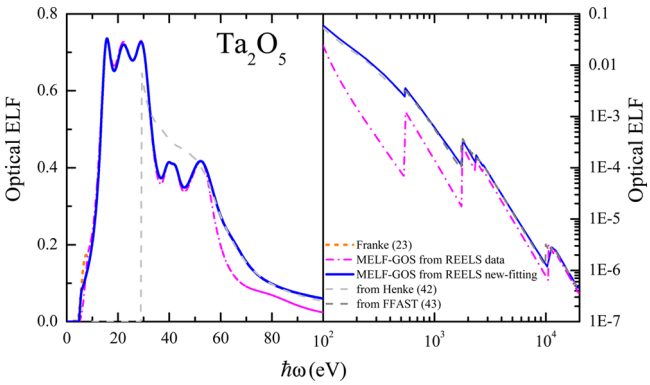

Figure 2. Optical energy loss function of Ta_2O_5 as a function of the transferred energy $\hbar\omega$. The left panel corresponds to the ELF at low transferred energy ($\hbar\omega \leq 100$ eV), whereas the right panel (on a logarithmic scale) depicts the ELF due to excitations at intermediate and high energies. The magenta dash-dotted line is the ELF calculated with eq 2 and the parameters given in Table 1, derived from the REELS original data shown in Figure 1. The blue solid line represents the improved ELF based on the parameters of Table 2, derived from the MELF-GOS method with the requirement of the *f*-sum rule fulfillment. The light and dark gray dashed lines result from the atomic scattering factors taken from X-ray data[42] and more recent calculations,[43] and the orange dots (at very low energy) represent experimental data.[23]

We can observe in Figure 2 that the ELF of Ta_2O_5 presents a small shoulder at 7.9 eV, due to electron transitions from valence band into conduction band, several well-defined peaks at 15.6, 22.2, and 28.8 eV, which can be attributed to plasma oscillations of valence electrons and/or to interband transitions, and broad peaks at 40.4 and 52.2 eV, which can be related to electronic interband transitions of the d-electrons. After these energies, the ELF decreases smoothly to enter the inner-shell excitation region, where sharp discontinuities appear at the oxygen K-shell threshold (543.1 eV) and the K- (67416.1 eV), L- (11682 eV, 10508.6 eV), and M- (2708 eV, 2331.4 eV, 1764 eV) shell thresholds of Ta.

IV. THEORETICAL CALCULATION OF THE ENERGY LOSS OF SWIFT IONS IN SOLIDS: DIELECTRIC FORMALISM

Intimately related to the ELF of a material is the energy lost by swift projectiles due to electronic excitations induced during their passage through the medium. The dielectric formalism,[46−49] which is based on a perturbative analysis of the response of an absorbing medium to an external excitation, becomes a suitable method to evaluate the main energy loss magnitudes in a broad range of incident energies.

For an energetic ion with kinetic energy T, mass M, atomic number Z_1 and charge q that interacts with a medium, whose electronic excitation spectrum is represented by its energy loss function $\mathrm{Im}[-1/\varepsilon(k,\omega)]$, the target stopping power is given by[33]

$$S_q = \frac{Me^2}{\pi T}\int_0^\infty \frac{\mathrm{d}k}{k}\rho_q^2(k)\int_0^{k\sqrt{2T/M}} \mathrm{d}\omega\omega\mathrm{Im}\left[\frac{-1}{\varepsilon(k,\omega)}\right] \quad (7)$$

where $\rho_q(k)$ is the Fourier transform of the projectile charge density for the charge state q, which is calculated using the statistical Brandt−Kitagawa model.[50,51]

DOI: 10.1021/acs.jpcc.5b04292
J. Phys. Chem. C XXXX, XXX, XXX−XXX

Taking into account that the charge state of the projectile changes dynamically due to electron capture and loss processes within the stopping material, then the total stopping power S can be written as

$$S = \sum_{q=0}^{Z_1} \phi_q S_q \tag{8}$$

where the equilibrium charge-state fractions ϕ_q represent the probability of finding the projectile in a given charge state q, which depends on its energy T and the target nature. These values are obtained from a parametrization of the experimental data,[52] which uses Bragg's additivity rule for compound targets. The summation in eq 8 extends over all possible charge states q of the projectile. Note that, in the stopping power calculation S_q, eq 7, the contribution due to the projectile polarization by the electric field induced in the target[53−55] and the energy loss produced in electron capture and loss events[53,56] are also included. A useful quantity to compare with experimental data is the stopping cross section (SCS), defined as the stopping power divided by the density of the target.

Fluctuations in the projectile energy loss due to the stochastic behavior of inelastic collisions are accounted for by the energy-loss straggling, Ω^2, which represents the variance of the projectile energy loss distribution per unit path length. In the dielectric formalism, Ω^2 is given by

$$\Omega^2 = \sum_{q=0}^{Z_1} \phi_q {\Omega_q}^2 = \frac{M\hbar e^2}{\pi T} \sum_{q=0}^{Z_1} \phi_q \int_0^\infty \frac{\mathrm{d}k}{k} {\rho_q}^2(k) \times \int_0^{k\sqrt{2T/M}} \mathrm{d}\omega\omega^2 \mathrm{Im}\left[\frac{-1}{\varepsilon(k,\omega)}\right] \tag{9}$$

where ${\Omega_q}^2$ is the energy-loss straggling of a projectile with charge state q. As in the case of the stopping power, the total energy-loss straggling Ω^2 is calculated as a weighted sum of ${\Omega_q}^2$ for the different charge states q of the projectile.

An important magnitude that enters into the Bethe formula[49,57,58] at high incident projectile energies is the mean excitation energy I of the target,[58,59] which can be obtained from the energy loss function as follows:

$$\ln I = \frac{\int_0^\infty \omega \ln(\omega) \mathrm{Im}[-1/\varepsilon(k=0,\omega)]\mathrm{d}\omega}{\int_0^\infty \omega \mathrm{Im}[-1/\varepsilon(k=0,\omega)]\mathrm{d}\omega} \tag{10}$$

The resulting value for Ta_2O_5 is I = 461.9 eV, which is sensibly lower than the value 523.8 eV obtained by the procedure based in the Bragg rule outlined in the ICRU Report 49.[60]

V. EXPERIMENTAL DETERMINATION OF THE ENERGY LOSS OF H AND He IONS IN Ta_2O_5 FILMS

A. Preparation and Characterization of Ta_2O_5 Films. The Ta_2O_5 films were grown on a Si(100) substrate by radio frequency magnetron sputtering (300 W) using a commercial Ta_2O_5 target and an O_2/Ar mixture as sputtering gas. The base pressure was 5.0×10^{-7} Torr, and the Ar^+/O_2 pressure during deposition was 5.3 mTorr. A Rigaku θ−2θ diffractometer employing Cu K-α radiation was utilized to obtain low- and high-angle diffraction scans. The thickness of each film was derived from the deposition time and a growth rate of about 2.8 nm/min. It was measured afterward using the X-ray reflectivity technique and the software package WinGixa from Philips.[61,62] Besides the thickness, the root-mean-square roughness and mass density of each film were deduced from the fits. The thicknesses t of the Ta_2O_5 films were 25 (1), 36 (1), 45 (1), 58 (1), 75 (1), 95 (2), 110 (3), and 173 (3) nm. The roughness was 0.5 nm for films with $t \leq 95$ nm, and the average mass density was 8.22 (0.06) g/cm^3, where the uncertainty was given by the standard deviation of the density values in the fits. For films with t = 110 and 173 nm, in which the use of the reflectivity technique is not appropriate, their thicknesses were estimated by comparing the widths of the Ta structure in the Rutherford backscattering (RBS) spectra with the respective ones obtained for thinner films. It should be stressed that these films were not used in the energy-loss straggling experiments due to the lack of information on their roughness. Measured and fitted X-ray reflectivity spectra are shown in Figure 3 for several thicknesses of the Ta_2O_5 films. A good agreement was found between the experiment (symbols) and simulation (solid lines) of the reflectivity. The stoichiometry of the films was checked and confirmed by the RBS measurements.

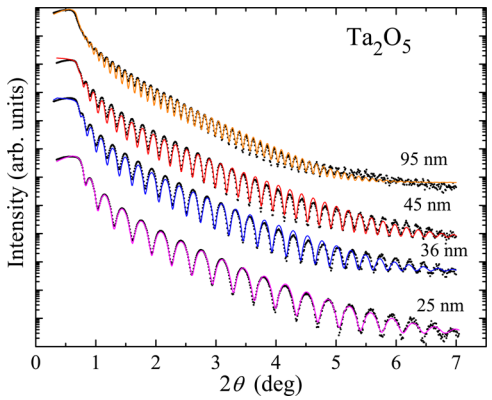

Figure 3. Measured X-ray reflectivity spectra (symbols) and corresponding WinGIXA simulated spectra (solid curves) for four Si(100)/Ta_2O_5 films, labeled with the corresponding thickness of the Ta_2O_5 films.

B. Measurement of the SCS and the Energy-Loss Straggling by Using the Rutherford Backscattering Technique. The energy loss measurements were performed at the Instituto de Física da Universidade Federal do Rio Grande do Sul, Brazil, with H^+ and He^+ ion beams delivered by the 500 kV ion implanter for the lower energies, and a 3 MV tandem accelerator for the higher ones. The samples deposited on a Si wafer were mounted on a four-axis goniometer. For each ion beam energy, a sample thickness was selected such that the Ta structure in the RBS spectrum will be well-defined. In some cases two different samples were analyzed at the same energy, and the obtained results were quite compatible.

The RBS measurements for the stopping power were done with the detector fixed at θ = 120° with respect to the beam direction. For each beam energy, four spectra were recorded at the incidence angles θ_1 of 0°, 20°, 40°, and 60° between the sample normal and the beam direction. The RBS spectra were acquired with a Si surface barrier detector. The overall resolution of the detector plus the associated electronics was 8 keV for H and around 13 keV for He. The covered energy ranges were 300−2000 keV for H, and 200−6000 keV for He. Typical experimental RBS spectra are displayed in Figure 4a for 400 keV H at the incidence angle θ_1 = 0° on 74.5 nm Ta_2O_5, where symbols represent current measurements, whereas the continuous curve stands for the fitting of the Ta structure.

DOI: 10.1021/acs.jpcc.5b04292
J. Phys. Chem. C XXXX, XXX, XXX−XXX

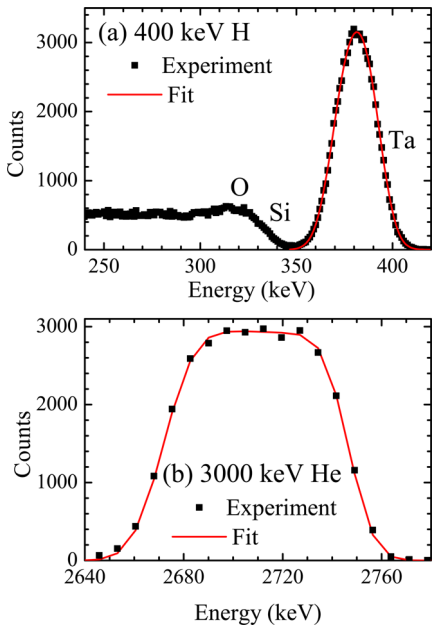

Figure 4. (a) RBS spectrum (symbols) used to extract the Ta_2O_5 stopping cross section: a 74.5 nm Ta_2O_5 film bombarded by a 400 keV H beam at normal incidence. It is possible to see the O signal from the film, as well as the Si structure from the substrate. (b) RBS spectrum used to extract the energy-loss straggling of Ta_2O_5: a 94.5 nm Ta_2O_5 film was bombarded by a 3000 keV He beam at the incidence angle of $\theta_1 = 45°$. In both cases, symbols correspond to present RBS measurements, whereas the solid lines represent the fit to the Ta signal.

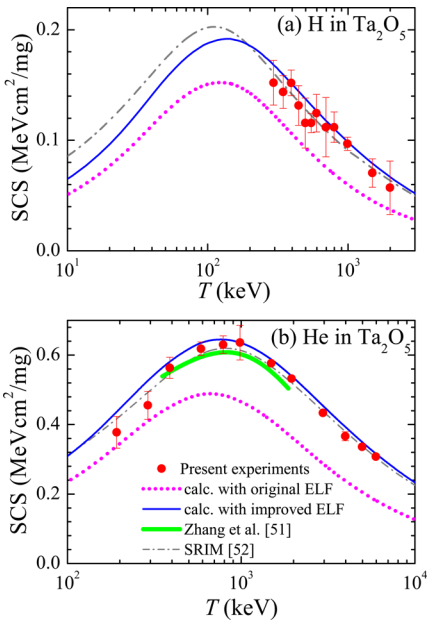

Figure 5. Stopping cross section (SCS) of Ta_2O_5 for (a) protons and (b) helium ions, as a function of the incident projectile energy T. Experimental data obtained in this work are shown by symbols, with their corresponding error bars. The blue solid lines represent calculations from the dielectric formalism using as input the improved ELF of Ta_2O_5, whereas the magenta dotted line was obtained from the dielectric formalism when using the ELF directly extracted from the REELS data. A gray dash-dotted line depicts the results of the semiempirical SRIM code.[67] Experimental data obtained for helium ions with the transmission technique[66] are represented by a thick green line.

For the energy-loss straggling measurements, we have used only the films with $t \leq 94.5$ nm since they have a well determined roughness at the interface with the Si substrate. A wide energy interval was covered in the present experiment: 200−1500 keV for H and 400−4000 keV for He ions. For each incident ion energy, we have used the appropriate film and the spectra were recorded at 0°, 30° and 45° between the normal and the incident ion beam, in order to have better precision in our final results. Typical results for 3000 keV He are shown in Figure 4b for a 94.5 nm Ta_2O_5 film at 45° with respect to the beam. The full line is the fitting to the Ta signal.

A careful analysis of the RBS spectra was done by applying the fundamentals of the RBS technique,[36,63,64] from which the stopping cross sections were extracted with an estimated error of the order of 10% for H and less than 6% for He. It should be stressed that the stopping cross section determination requires at least two independent measurements at different beam-sample angles. However, we have performed the experiments at four angles in order to improve the precision of the obtained results. For a detailed explanation of the present procedure, see ref 36.

On the other hand, in order to determine the energy-loss straggling values from the experimental spectra, we have followed a procedure already described,[65] which in turn is based on the algorithm proposed by Chu et al.[63]

In Figure 5, we show the stopping cross section (SCS) of Ta_2O_5 for (a) protons and (b) α particle beams, as a function of the incident energy. Symbols represent the results obtained from the present measurements. The data corresponding to He ions are in very good agreement with the available experimental data around the maximum of the SCS (thick green line), which were obtained using the transmission technique.[66] Blue solid lines represent the SCS calculated with the dielectric formalism when using the improved ELF of Ta_2O_5, as explained in section IV. As it can be seen, there is a quite good agreement in the wide ion energy region where experimental data are available, for protons as well as helium ion beams. If we use for the outer-shell electron excitations the ELF originally obtained from REELS in section II, together with the GOS extension to account for inner-shell contributions to the ELF, then the magenta dotted curves result, which substantially differ from the experimental SCS and energy-loss straggling. For comparison purposes, the results obtained from the semi-empirical SRIM code[67] are also shown in the figure by gray dash-dotted lines.

Figure 6 shows the experimental and calculated energy-loss straggling values for H and He beams in Ta_2O_5 films, as a function of the ion energy. Experimental results are depicted in the figures by symbols. For the H beam, the measured range interval covers from 200 to 1500 keV, while for He it ranges between 400 and 4000 keV. Theoretical results obtained from the dielectric formalism, eq 9, with both the improved and the originally derived ELF from REELS, are presented by a solid blue line and a magenta dotted line, respectively. Similarly to the stopping cross section results, the experimental-theoretical agreement of the energy-loss straggling is excellent when using the improved ELF derived in section III. The horizontal dashed lines in Figure 6 represent Bohr's energy-loss straggling Ω_B^2, which, for a compound target as Ta_2O_5, is obtained in a first-order approximation by the addition of the $(\Omega_{B,j}^2/N_j)$ ratios, where $\Omega_{B,j}^2 = 4\pi Z_1^2 Z_2 e^4 N_j$ is the Bohr energy-loss straggling[68] of each one of the compound j-atomic constituent.[65]

DOI: 10.1021/acs.jpcc.5b04292
J. Phys. Chem. C XXXX, XXX, XXX−XXX

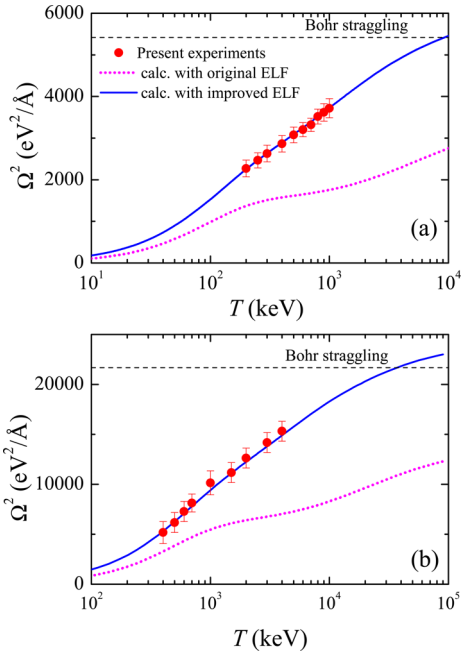

Figure 6. Energy-loss straggling Ω^2 of (a) protons and (b) alpha particles in Ta_2O_5. Symbols correspond to present experimental measurements obtained with the RBS technique. Lines are calculations from the dielectric formalism using the improved ELF (blue solid line) and the originally derived ELF from REELS (magenta dotted line). The horizontal black dashed line corresponds to the Bohr energy-loss straggling, Ω_B^2.

The excellent agreement of the experimental SCS and the energy-loss straggling with the corresponding calculations using the improved ELF (derived in section III), as compared to the originally ELF deduced from REELS (see section II) is taken as a validation criterion to use for Ta_2O_5 the ELF represented in Figure 2, obtained from eqs 4 and 5 with the parameters given in Table 2.

VI. INELASTIC MEAN FREE PATH AND STOPPING POWER OF SWIFT ELECTRON BEAMS

The reliability of the improved ELF obtained in section III is assessed by the excellent agreement between the theoretical and the experimental stopping cross sections as well as the energy-loss straggling of Ta_2O_5 for H and He ion beams. Therefore, we will apply this ELF to obtain the inelastic mean free path (IMFP) and the stopping power of electrons in Ta_2O_5, which are relevant quantities for characterization and modification of solid media by means of electron beam techniques such as electron microscopy, X-ray photoelectron, Auger electron spectroscopy and related techniques.[4,69,70] Besides, the electron IMFP and stopping power are essential inputs in the simulation of electron transport in solids with Monte Carlo method.[71]

If we consider a nonrelativistic electron with kinetic energy T, the dielectric formalism gives the following expressions for the inverse IMFP, λ^{-1}, and the stopping power S_e in a solid:[34,72]

$$\lambda_e^{-1} = \frac{me^2}{\hbar\pi T}\int_0^{W_{max}} d\omega \int_{k_1}^{k_2} \frac{dk}{k}[1 + f_{ex}(k)]\mathrm{Im}\left[\frac{-1}{\varepsilon(k,\omega)}\right] \quad (11)$$

and

$$S_e = \frac{me^2}{\pi T}\int_0^{W_{max}} d\omega\omega \int_{k_1}^{k_2} \frac{dk}{k}[1 + f_{ex}(k)]\mathrm{Im}\left[\frac{-1}{\varepsilon(k,\omega)}\right] \quad (12)$$

where the integration limits $k_{1,2}$ are given in section II. The maximum transferred energy $\hbar W_{max}$ by an electron with energy T cannot exceed the value $T - E_{gap}$, where E_{gap} is the target band gap energy. Besides, the indistinguishability between the incident electron and a generated secondary electron means that the maximum energy transfer cannot exceed $T/2$. Therefore, the maximum transferred energy will be given by $\hbar W_{max} = \min(T/2, T - E_{gap})$. Finally, the exchange effects in the electron−electron interaction due to the indistinguishability of scattered and ejected electrons must be considered when the energy of both electrons are similar; to account for this effect, we include the exchange corrections given by the Ochkur approximation,[73] where the exchange term is $f_{ex}(k) = (\hbar k/mv)^4 - (\hbar k/mv)^2$, where v is the velocity of the incident electron. The Pauli exclusion principle is considered in all the cases.

The inelastic mean free path λ and the stopping cross section SCS for electrons are depicted in Figure 7 as a function of the electron kinetic energy. The blue solid lines represent calculations obtained from the improved ELF, whereas the magenta dotted lines were obtained using the ELF originally deduced from REELS. Differences between both procedures are larger at higher electron energies, especially for the stopping cross section at energies around and larger than the maximum of the SCS. Mean free path and stopping power measurements are required at high and intermediate electron energies in order to elucidate the discrepancy between both ELF models due to the contribution of the target electron excitations at intermediate and high energies. Besides, the IMFP at large energies is crucial in the interpretation of hard X-ray photoemission spectroscopy (HAXPES), and therefore, a precise knowledge of the IMFP at high energies is of real interest.[74,75]

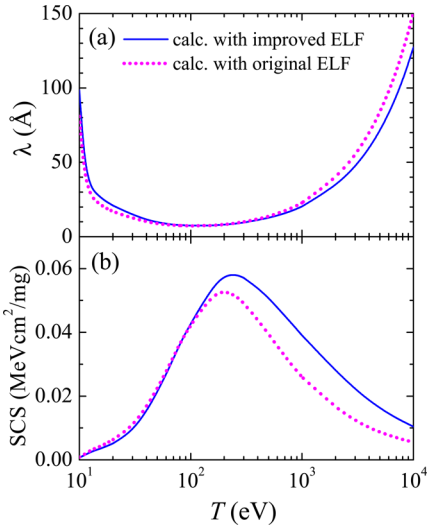

Figure 7. Dielectric formalism results for (a) the inelastic mean free path, λ, and (b) the stopping cross section (SCS) of electrons in Ta_2O_5, as a function of the incident electron energy T. Blue solid lines correspond to the results obtained when using the improved ELF (section III), whereas the magenta dotted lines come from the use of the ELF originally derived from REELS (section II).

DOI: 10.1021/acs.jpcc.5b04292
J. Phys. Chem. C XXXX, XXX, XXX−XXX

VII. SUMMARY AND CONCLUSIONS

In the present, work we have performed a joint experimental-theoretical study to reliably determine the energy loss function (ELF) of Ta_2O_5, which is a magnitude that enters as a main ingredient in numerous areas of materials science.

The target outer shell electron excitations contribution to the ELF was initially derived from reflection electron energy loss spectrocopy measurements. Then this ELF was further improved theoretically, through the MELF-GOS methodology, by the proper inclusion of the inner-shell electrons contribution and requiring the fulfillment of physically motivated sum rules, as the KK- and the *f*-sum rule. The dielectric formalism applied to the calculated ELF provided the stopping cross sections and energy-loss straggling of Ta_2O_5 for proton and α particle beams. These magnitudes were experimentally determined for a broad range of incident projectile energies by using the Rutherford backscattering methodology. The reliability of the Ta_2O_5 ELF deduced in this work is assessed by the excellent agreement between the measured SCS and energy-loss straggling as compared with the corresponding calculations obtained by means of the dielectric formalism. As a further result of our study, we have calculated the inelastic mean free path and the stopping cross sections of swift electrons in Ta_2O_5, both magnitudes being of relevance in further studies of this promising material in the microelectronics industry.

In conclusion, we have derived a realistic ELF for Ta_2O_5, taking into account chemical and phase effects, which is valid for all momentum and energy transfers. For this purpose, we have used different (and complementary) experimental and theoretical procedures, to improve and evaluate the results. Thus, we have shown how an ELF experimentally derived from REELS measurements can be further improved by applying theoretical considerations. Finally, the reliability of the ELF has been assessed by independent measurements through the Rutherford backscattering method of the stopping cross sections and the energy-loss straggling of swift H and He beams in Ta_2O_5.

AUTHOR INFORMATION

Corresponding Author

*Mailing address: Departament de Física Aplicada, Universitat d'Alacant, E-03080 Alacant, Spain. Tel. +34 965909578. E-mail: ias@ua.es.

Notes

The authors declare no competing financial interest.

ACKNOWLEDGMENTS

The authors wish to thank the Crystallographic Laboratory of Physics-USP for the use of X-ray diffraction. We acknowledge financial support from the Brazilian agencies Coordinação de Aperfeiçoamento de Pessoal de Nivel Superior (CAPES), Conselho Nacional de Desenvolvimento Científico e Tecnológico (CNPq) and PRONEX-FAPERGS, as well as the Australian Research Council and the Spanish Ministerio de Economía y Competitividad (Project FIS2014-58849-P).

REFERENCES

(1) Werner, W. S. M.; Glantschnig, K.; Ambrosch-Draxi, C. Optical Constants and Inelastic Electron-Scattering Data for 17 Elemental Metals. *J. Phys. Chem. Ref. Data* **2009**, *38*, 1013−1092.

(2) Egerton, R. F. Electron Energy-Loss Spectroscopy in the TEM. *Rep. Prog. Phys.* **2009**, *72*, 016502.

(3) Da, B.; Shinotsuka, H.; Yoshikawa, H.; Ding, Z. J.; Tanuma, S. Extended Mermin Method for Calculating the Electron Inelastic Mean Free Path. *Phys. Rev. Lett.* **2014**, *113*, 063201.

(4) Egerton, R. F. *Electron Energy-Loss Spectroscopy in the Electron Microscope*, 3rd ed.; Springer: New York, 2011.

(5) Ritsko, J. J.; Brillson, L. J.; Bigelow, R. W.; Fabish, T. J. Electron Energy Loss Spectroscopy and the Optical Propeties of Polymethylmethacrylate from 1 to 300 eV. *J. Chem. Phys.* **1978**, *69*, 3931−3939.

(6) Frandon, J.; Brousseau, B.; Pradal, F. Electronic Excitations in some Transition Metals and their Oxides. *Phys. Status Solidi B* **1980**, *98*, 379−385.

(7) Hayashi, H.; Watanabe, N.; Udagawa, Y.; Kao, C.-C. Optical Spectra of Liquid Water in Vacuum UV Region by Means of Inelastic X-Ray Scattering Spectroscopy. *J. Chem. Phys.* **1998**, *108*, 823−825.

(8) Fuentes, G. G.; Mancheño, I. G.; Balbás, F.; Quirós, C.; Trigo, J. F.; Yubero, F.; Elizalde, E.; Sanz, J. M. Dielectric Properties of Ti, TiO_2 and TiN from 1.5 to 60 eV Determined by Reflection Electron Energy Loss Spectroscopy (REELS) and Ellipsometry. *Phys. Status Solidi A* **1999**, *175*, 429−436.

(9) Jin, H.; Oh, S. K.; Kang, H. J.; Tougaard, S. Electronic Properties of Ultrathin HfO_2, Al_2O_3, and Hf−Al−O Dielectric Films on Si (100) Studied by Quantitative Analysis of Reflection Electron Energy Loss Spectra. *J. Appl. Phys.* **2006**, *100*, 083713.

(10) Vos, M.; Grande, P. L. The Relation Between the Electron Energy Loss Spectra of Hafnia and its Dielectric Function. *Surf. Sci.* **2014**, *630*, 1−8.

(11) Abril, I.; Garcia-Molina, R.; Denton, C. D.; Pérez-Pérez, F. J.; Arista, N. R. Dielectric Description of Wakes and Stopping Powers in Solids. *Phys. Rev. A: At., Mol., Opt. Phys.* **1998**, *58*, 357−366.

(12) Heredia-Avalos, S.; Garcia-Molina, R.; Fernández-Varea, J. M.; Abril, I. Calculated Energy Loss of Swift He, Li, B, and N Ions in SiO_2, Al_2O_3, and ZrO_2. *Phys. Rev. A: At., Mol., Opt. Phys.* **2005**, *72*, 052902.

(13) Bourke, J. D.; Chantler, C. T. Momentum-Dependent Lifetime Broadening of Electron Energy Loss Spectra: A Self-consistent Coupled-Plasmon Model. *J. Phys. Chem. Lett.* **2015**, *6*, 314−319.

(14) Nguyen-Truong, H. T. Penn Algorithm Including Damping for Calculating the Electron Inelastic Mean Free Path. *J. Phys. Chem. C* **2015**, *119*, 7883−7887.

(15) Shiles, E.; Sasaki, T.; Inokuti, M.; Smith, D. Y. Self-Consistency and Sum-Rule Test in the Kramers-Kroning Analysis of Optical Data: Applications to Aluminum. *Phys. Rev. B: Condens. Matter Mater. Phys.* **1980**, *22*, 1612−1628.

(16) Doumuki, T.; Tamada, H.; Saitoh, M. Highly Efficient Cherenkov-type Second Harmonic Generation in a Ta_2O_5/$KTiOPO_4$ Waveguide. *Appl. Phys. Lett.* **1994**, *64*, 353−355.

(17) Lee, M.-J.; Lee, C. B.; Lee, D.; Lee, S. R.; Chang, M.; Hur, J. H.; Kim, Y.-B.; Kim, C.-J.; Seo, D. H.; Seo, S.; et al. A Fast, High-endurance and Scalable Non-volatile Memory Device Made from Asymmetric Ta_2O_{5-x}/TaO_{2-x} Bilayer Structures. *Nat. Mater.* **2011**, *10*, 625−630.

(18) Nashed, R.; Hassan, W. M. I.; Ismail, Y.; Allam, N. K. Unravelling the Interplay of Crystal Structure and Electronic Band Structure of Tantalum Oxide (Ta_2O_5). *Phys. Chem. Chem. Phys.* **2013**, *15*, 1352−1357.

(19) Park, G.-S.; Kim, Y. B.; Park, S. Y.; Li, X. S.; Heo, S.; Lee, M.-J.; Chang, M.; Kwon, J. H.; Kim, M.; Chung, U.-I.; et al. In Situ Observation of Filamentary Conducting Channels in an Asymmetric Ta_2O_{5-x}/TaO_{2-x} Bilayer Structure. *Nat. Commun.* **2013**, *4*, 2382.

(20) Postava, K.; Aoyama, M.; Yamaguchi, T.; Oda, H. Spectroellipsometric Characterization of Materials for Multilayer Coating. *Appl. Surf. Sci.* **2001**, *175*−*176*, 276−280.

(21) Azim, O. A.; Abdel-Aziz, M. M.; Yahia, I. S. Structure and Optical Analysis of Ta_2O_5 Deposited on Infrasil Substrate. *Appl. Surf. Sci.* **2009**, *255*, 4829−4835.

(22) Sharlandjiev, P. S.; Nazarova, D. I. Determination of Optical Functions of Very Thin Tantalum Pentoxide Films on Platinum Substrate by Genetic Algorithm Approach. *Opt. Quantum Electron.* **2012**, *44*, 673−681.

DOI: 10.1021/acs.jpcc.5b04292
J. Phys. Chem. C XXXX, XXX, XXX−XXX

(23) Franke, E.; Trimble, C. L.; DeVries, M. J.; Woollam, J. A.; Schubert, M.; Frost, F. Dielectric Function of Amorphous Tantalum Oxide from the Far Infrared to the Deep Ultraviolet Spectral Region Measured by Spectroscopic Ellipsometry. *J. Appl. Phys.* **2000**, *88*, 5166−5174.
(24) Hajati, S.; Romanyuk, O.; Zemek, J.; Tougaard, S. Validity of Yubero-Tougaard Theory to Quantitatively Determine the Dielectric Properties of Surface Nanofilms. *Phys. Rev. B: Condens. Matter Mater. Phys.* **2008**, *77*, 155403.
(25) Shvets, V. A.; Aliev, V., Sh; Gritsenko, D. V.; Shaimeev, S. S.; Fedosenko, E. V.; Rykhlitski, S. V.; Atuchin, V. V.; Gritsenko, V. A.; Tapilin, V. M.; Wong, H. Electronic Structure and Charge Transport Properties of Amorphous Ta_2O_5 Films. *J. Non-Cryst. Solids* **2008**, *354*, 3025−3033.
(26) Vos, M.; Grande, P. L. High-Energy Electron Scattering from TiO_2 Surfaces. *Nucl. Instrum. Methods Phys. Res., Sect. B* **2015**, *354*, 332−339.
(27) Tougaard, S.; Chorkendorff, I. Differential Inelastic Electron-Scattering Cross Sections from Experimental Reflection Electron-Energy-Loss spectra−Application to Background Removal in Electron-Spectroscopy. *Phys. Rev. B: Condens. Matter Mater. Phys.* **1987**, *35*, 6570−6577.
(28) Tougaard, S.; Yubero, F. QUEELS Software Package for Calculation of Surface Effects in Electron Spectra. *Surf. Interface Anal.* **2004**, *36*, 824−827.
(29) Pines, D.; Nozières, P. *The Theory of Quantum Liquids*; Benjamin, New York, 1966; Vol. *1*.
(30) Tanuma, S.; Powell, C. J.; Penn, D. R. Use of Sum Rules on the Energy-Loss Function for the Evaluation of Experimental Optical Data. *J. Electron Spectrosc. Relat. Phenom.* **1993**, *62*, 95−109.
(31) Gao, L.; Lemarchand, F.; Lequime, M. Exploitation of Multiple Incidences Spectrometric Measurements for Thin Film Reverse Engineering. *Opt. Express* **2012**, *20*, 15734−15751.
(32) Chaneliere, C.; Autran, J. L.; Devine, R. A. B.; Balland, B. Tantalum Pentoxide (Ta_2Os) Thin Films for Advanced Dielectric Applications. *Mater. Sci. Eng., R* **1998**, *22*, 269−322.
(33) Garcia-Molina, R.; Abril, I.; Kyriakou, I.; Emfietzoglou, D. Energy Loss of Swift Protons in Liquid Water: Role of Optical Data Input and Extension Algorithms. In *Radiation Damage in Biomolecular Systems*; García Gómez-Tejedor, G., Fuss, M. C., Eds.; Springer, Dordrecht, 2012; Chapter 15.
(34) Behar, M.; Fadanelli, R. C.; Abril, I.; Garcia-Molina, R.; Denton, C. D.; Nagamine, L. C. C. M.; Arista, N. R. Energy Loss of Proton, α-particle, and Electron Beams in Hafnium Dioxide Films. *Phys. Rev. A: At., Mol., Opt. Phys.* **2009**, *80*, 062901.
(35) Behar, M.; Denton, C. D.; Fadanelli, R. C.; Abril, I.; Cantero, E. D.; Garcia-Molina, R.; Nagamine, L. C. C. M. Experimental and Theoretical Determination of the Stopping Power of ZrO_2 Films for Protons and α-particles. *Eur. Phys. J. D* **2010**, *59*, 209−213.
(36) Limandri, S. P.; Fadanelli, R. C.; Behar, M.; Nagamine, L. C. C. M.; Fernández-Varea, J. M.; Abril, I.; Garcia-Molina, R.; Montanari, C. C.; Aguiar, J. C.; Mitnik, D.; et al. Stopping Cross Sections of TiO_2 for H and He Ions. *Eur. Phys. J. D* **2014**, *68*, 194.
(37) Bourke, J. D.; Chantler, C. T. Electron Energy Loss Spectra and Overestimation of Inelastic Mean Free Paths in Many-Poles Models. *J. Phys. Chem. A* **2012**, *116*, 3202.
(38) Mermin, N. D. Lindhard Dielectric Function in the Relaxation Time Approximation. *Phys. Rev. B* **1970**, *1*, 2362−2363.
(39) Heredia-Avalos, S.; Moreno-Marín, J. C.; Abril, I.; Garcia-Molina, R. Energy Loss of H^+ and He^+ in the Semiconductors GaAs, ZnSe, InP and SiC. *Nucl. Instrum. Methods Phys. Res., Sect. B* **2005**, *230*, 118−124.
(40) Planes, D. J.; Garcia-Molina, R.; Abril, I.; Arista, N. R. Wavenumber Dependence of the Energy Loss Function of Graphite and Aluminum. *J. Electron Spectrosc. Relat. Phenom.* **1996**, *82*, 23−29.
(41) Garcia-Molina, R.; Abril, I.; Denton, C. D.; Heredia-Avalos, S.; Kyriakou, I.; Emfietzoglou, D. Calculated Depth-Dose Distributions for H^+ and He^+ Beams in Liquid Water. *Nucl. Instrum. Methods Phys. Res., Sect. B* **2009**, *267*, 2647−2652.
(42) Henke, B. L.; Gullikson, E. M.; Davis, J. C. X-Ray Interactions: Photoabsorption, Scattering, Transmission, and Reflection at E = 50−30000 eV, Z = 1−92. *At. Data Nucl. Data Tables* **1993**, *54*, 181−342.
(43) Chantler, C. T.; Olsen, K.; Dragoset, R. A.; Chang, J.; Kishore, A. R.; Kotochigova, S. A.; Zucker, D. S. *X-Ray Form Factor, Attenuation and Scattering Tables* (version 2.1); National Institute of Standards and Technology: Gaithersburg, MD, 2005; online available: http://physics.nist.gov/ffast.
(44) Chantler, C. T. Detailed Tabulation of Atomic Form Factors, Photoelectric Absorption and Scattering Cross Section, and Mass Attenuation Coefficients in the Vicinity of Absorption Edges in the Soft X-Ray (Z = 30−36, Z = 60−89, E = 0.1 keV-10 keV), Addressing Convergence Issues of Earlier Work. *J. Phys. Chem. Ref. Data* **2000**, *29*, 597−1048.
(45) Chantler, C. T. Theoretical Form Factor, Attenuation and Scattering Tabulation for Z = 1−92 from E = 1−10 eV to E = 0.4−1.0 MeV. *J. Phys. Chem. Ref. Data* **1995**, *24*, 71−643.
(46) Fermi, E. The Ionization Loss of Energy in Gases and in Condensed Materials. *Phys. Rev.* **1940**, *57*, 485−493.
(47) Lindhard, J. On the Properties of a Gas of Charged Particles. *K. Dan. Vidensk. Selsk. Mater.-Fys. Medd.* **1954**, *28* (8), 1−57.
(48) Ritchie, R. H. Interaction of Charged Particles with a Degenerate Fermi−Dirac Electron Gas. *Phys. Rev.* **1959**, *114*, 644−654.
(49) Sigmund, P. *Particle Penetration and Radiation Effects. General Aspects and Stopping of Swift Point Charges*; Springer Series in Solid State Sciences, Vol. *151*; Springer: Berlin, 2006.
(50) Brandt, W.; Kitagawa, M. Effective Stopping-Power Charges of Swift Ions in Condensed Matter. *Phys. Rev. B: Condens. Matter Mater. Phys.* **1982**, *25*, 5631−5637.
(51) Brandt, W. Effective Charges of Ions and the Stopping Power of Dense Media. *Nucl. Instrum. Methods Phys. Res.* **1982**, *194*, 13−19.
(52) Schiwietz, G.; Grande, P. L. Improved Charge-State Formulas. *Nucl. Instrum. Methods Phys. Res., Sect. B* **2001**, *175−177*, 125−131.
(53) Heredia-Avalos, S.; Garcia-Molina, R. Projectile Polarization Effects in the Energy Loss of Swift Ions in Solids. *Nucl. Instrum. Methods Phys. Res., Sect. B* **2002**, *193*, 15−19.
(54) Moreno-Marín, J. C.; Abril, I.; Heredia-Avalos, S.; Garcia-Molina, R. Electronic Energy Loss of Swift H^+ and He^+ Ions in Solids with Material Science Applications. *Nucl. Instrum. Methods Phys. Res., Sect. B* **2006**, *249*, 29−33.
(55) Heredia-Avalos, S.; Abril, I.; Denton, C. D.; Moreno-Marín, J. C.; Garcia-Molina, R. Target Inner-Shells Contributions to the Stopping Power and Straggling for H and He Ions in Gold. *J. Phys.: Condens. Matter* **2007**, *19*, 466205.
(56) Denton, C. D.; Abril, I.; Moreno-Marín, J. C.; Heredia-Avalos, S.; Garcia-Molina, R. Energy Loss of Swift H and He Projectiles in Al, Si, Ni and Cu Targets. *Phys. Status Solidi B* **2008**, *245*, 1498−1504.
(57) Bethe, H. The Theory of the Passage of Rapid Neutron Radiation through Matter. *Ann. Phys.* **1930**, *397*, 325−400.
(58) Inokuti, M. Inelastic Collisions of Fast Charged Particles with Atoms and Molecules − The Bethe Theory Revisited. *Rev. Mod. Phys.* **1971**, *43*, 297−347.
(59) Fano, U. Penetration of Protons, Alpha Particles, and Mesons. *Annu. Rev. Nucl. Sci.* **1963**, *13*, 1−66.
(60) ICRU. *Stopping Powers and Ranges for Protons and Alpha Particles*, Report 49; International Commission on Radiation Units and Measurements: Bethesda, MD, 1993.
(61) Leenaers, A. J. G.; de Boer, D. K. G. Applications of Glancing Incidence X-Ray Analysis. *X-Ray Spectrom.* **1997**, *26*, 115−121.
(62) Nagamine, L. C. C. M.; Biondo, A.; Pereira, L. G.; Mello, A.; Schmidt, J. E.; Chimendes, T. W.; Cunha, J. B. M.; Saitovitch, E. B. Effect of Interface Intermixing on Giant Magnetoresistance in NiFe/Cu and Co/NiFe/Co/Cu Multilayers. *J. Appl. Phys.* **2003**, *94*, 5881−5890.
(63) Chu, W. K.; Mayer, J. W.; Nicolet, M. A. *Backscattering Spectrometry*; Academic Press: New York, 1978.
(64) Lantschner, G. H.; Eckardt, J. C.; Lifschitz, A. F.; Arista, N. R.; Araujo, L. L.; Duarte, P. F.; dos Santos, J. H. R.; Behar, M.; Dias, J. F.;

DOI: 10.1021/acs.jpcc.5b04292
J. Phys. Chem. C XXXX, XXX, XXX−XXX

Grande, P. L.; et al. Energy Loss of Helium Ions in Zinc. *Phys. Rev. A: At., Mol., Opt. Phys.* **2004**, *69*, 062903.
(65) Abril, I.; Behar, M.; Garcia-Molina, R.; Fadanelli, R. C.; Nagamine, L. C. C. M.; Grande, P. L.; Schünemann, L.; Denton, C. D.; Arista, N. R.; Saitovitch, E. B. Experimental and Theoretical Studies of the Energy-Loss Straggling of H and He Ion Beams in HfO_2 Films. *Eur. Phys. J. D* **2009**, *54*, 65−70.
(66) Zhang, Y.; Weber, W. J.; Grove, D. A.; Jensen, J.; Possnert, G. Electronic Stopping Powers for Heavy Ions in Niobium and Tantalum Pentoxides. *Nucl. Instrum. Methods Phys. Res., Sect. B* **2006**, *250*, 62−65.
(67) Ziegler, J. F.; Biersack, J. P.; Ziegler, M. D. *SRIM The Stopping and Range of Ions in Matter*, 2008; code available at http://www.srim.org.
(68) Bohr, N. The Penetration of Atomic Particles through Matter. *K. Dan. Vidensk. Selsk. Mater. Fys. Medd.* **1948**, *18* (8), 1−114.
(69) Werner, W. S. M.; Smekal, W.; Stori, H.; Winter, H.; Stefani, G.; Ruocco, A.; Offi, F.; Gotter, R.; Morgante, A.; Tommasini, F. Emission-Depth-Selective Auger Photoelectron Coincidence Spectroscopy. *Phys. Rev. Lett.* **2005**, *94*, 038302.
(70) Powell, C. J.; Jablonski, A. Surface Sensitivity of X-Ray Photoelectron Spectroscopy. *Nucl. Instrum. Methods Phys. Res., Sect. A* **2009**, *601*, 54−65.
(71) Dapor, M. *Transport of Energetic Electrons in Solids: Computer Simulation with Applications to Materials Analysis and Characterization*; Springer Tracts in Modern Physics, Vol. *257*; Springer: Berlin, 2014.
(72) Tung, C. J.; Ashley, J. C.; Ritchie, R. H. Electron Inelastic Mean Free Paths and Energy Losses in Solids II: Electron Gas Statistical Model. *Surf. Sci.* **1979**, *81*, 427−439.
(73) Ochkur, V. I. The Born-Oppenheimer Method in the Theory of Atomic Collisions. *Sov. Phys. JETP-USSR* **1964**, *18*, 503−508.
(74) Tanuma, S.; Powell, C. J.; Penn, D. R. Calculations of Electron Inelastic Mean Free Paths. IX. Data for 41 Elemental Solids over the 50 eV to 30 keV Range. *Surf. Interface Anal.* **2011**, *43*, 689−713.
(75) Panaccione, G.; Kobayashi, K. Hard X-Ray Photoemission Spectroscopy: Variable Depth Analysis of Bulk, Surface and Interface Electronic Properties. *Surf. Sci.* **2012**, *606*, 125−129.

DOI: 10.1021/acs.jpcc.5b04292
J. Phys. Chem. C XXXX, XXX, XXX−XXX